https://doi.org/10.5194/egusphere-2026-321
Preprint. Discussion started: 4 February 2026

Technical note: Kinetically resolved volatile and redox fingerprints of geologic materials by TGA/DSC-MicroGC

Shuzhuang Wu[1,2*], Samuel L. Jaccard[2], Matthieu E. Galvez[2*]

[1]State Key Laboratory of Deep-sea Science and Intelligence Technology, Institute of Deep-sea Science and Engineering, Chinese Academy of Sciences, Sanya, China
[2]Institute of Earth Sciences, University of Lausanne, Lausanne, Switzerland

Correspondence to: Shuzhuang Wu (shuzhuangwu@gmail.com), Matthieu E. Galvez (matthieu.galvez@unil.ch)

Abstract. The biogeochemical cycles of carbon, oxygen and sulfur are fundamental interlinked, yet quantifying their speciation and reactivity within complex geological matrices remains a major analytical challenge. We present a novel integrated TGA/DSC-MicroGC system that simultaneously monitors mass loss, heat flow, and evolved gas composition during controlled heating. This approach kinetically resolves and quantifies distinct carbon and sulfur species through their unique thermal decomposition profiles. Furthermore, continuous monitoring of oxygen consumption provides a direct measure of a material's absolute redox capacity, yielding a kinetic fingerprint of its reducible components. Validation against geochemical standards and application to sediments from the Congo Basin and Lake Cadagno, reveal diagenetic transitions and paleoenvironmental fluxes that are invisible to conventional bulk methods. This integrated methodology provides a mechanistic, high-resolution view of electron-transfer processes in natural materials, providing a transformative tool for probing biogeochemical cycling, redox evolution and environmental reactivity across Earth systems.

1 Introduction

The fate of carbon (C), sulfur (S) in sediments depends not only on their bulk concentration, but on their molecular speciation and intrinsic reactivity (Alt and Shanks Iii, 2006; Galvez, 2020; Hayes and Waldbauer, 2006; Paytan et al., 1998). For example, the oxidative weathering of a gram of labile organic matter versus graphite, or of monosulfide versus pyrite, occur at distinct temperature different activation energies (Boudreau, 1992; Hemingway et al., 2018; Ordoñez et al., 2019; Sebag et al., 2016). Their combustion also differs in reaction enthalpy and O_2 demand, reflecting their specific bonding strength of each compound (Galvez and Jaccard, 2021). Existing analytical techniques are poorly suited to capture these key dimensions of reactivity. Standard methods, such as elemental analysis or X-ray fluorescence, quantify total C and S, but are blind to speciation(Berg et al., 2022; Carter et al., 2024; Salonen, 1979; Yoon et al., 2018; Zhao et al., 2020). Meanwhile, Rock-Eval, a cornerstone in organic petrology, provides bulk chemical and kinetic parameters for hydrocarbon generation(Espitalie et al., 1985), but has critical limitations; it focuses on the ramped pyrolysis and combustion of carbon-bearing materials, and only the latest, expensive, Rock Eval 7, extends to S speciation (Cohen-Sadon et al., 2022). Critically, it cannot directly link the thermal decomposition of specific compounds to the concurrent consumption of oxygen, a key process for quantifying redox reactions.

Recent advances, such as the high-temperature titration method of Galvez & Jaccard (Galvez and Jaccard, 2021), have successfully quantified the total redox capacity of natural samples, partially bridging the gap between compositional and redox characterization. However, the standard protocol was designed as an endpoint measurement and, as such, provides no kinetic resolution of the oxidation process, nor insight into the individual contributions of C, S, and iron (Fe) species to the overall oxygen demand.

Consequently, a major disconnect persists between our understanding of global redox cycles and our ability to characterize the kinetic heterogeneity and coupled redox behavior of the materials that drive them. To address this gap, an analytical approach is required that goes beyond bulk measurements, and provides a simultaneous, kinetically-resolved view of mass loss, heat flow, and gas evolution during progressive heating. We have developed such a platform: a novel integrated system combining thermogravimetric analysis (TGA), differential scanning calorimetry (DSC), and micro gas chromatography (MicroGC). This configuration enables real-time, correlated measurements of mass loss, heat flow, and the evolving composition of gases (e.g., O_2, CO_2, SO_2, H_2S, COS) throughout controlled thermal oxidation. Specifically, this integration enables two key innovations:

1) It enables the kinetic resolution and quantification of distinct C and S species based on their characteristic thermal decomposition profiles and activation energies.
2) It provides a continuous, kinetically-resolved measure of absolute redox capacity by directly monitoring oxygen consumption, yielding a unique “chemical and redox fingerprint” for each sample.

Together, these capabilities reveal diagenetic pathways and paleoenvironmental signatures in complex natural archives that remain inaccessible to conventional analytical techniques.

https://doi.org/10.5194/egusphere-2026-321
Preprint. Discussion started: 4 February 2026

2 Materials and Methods

2.1 Sample selection and preparation

As representative samples, we analyzed sediment materials containing C, S and hydrogen (H) from contrasting depositional environments: the Congo Basin (0°51'24.095"S and 19°48'29.08"E) and Lake Cadagno (46°33'01.7"N, 8°42'44.3"E). The Congo Basin is the world's second-largest river basin and home to the planet's largest tropical peatland complex, which constitutes an exceptional archive of coupled C and O_2 dynamics(Crezee et al., 2022; Garcin et al., 2022). Kinetic resolution of redox processes in these sediments provides novel insight into degradation pathways associated with peat burial and climate-driven shifts since the Last Glacial Maximum. In contrast, Lake Cadagno, a meromictic lake in Switzerland with a permanently anoxic deep layer, serves as an ideal natural laboratory for studying microbial redox processes and their long-term preservation in the sedimentary record (Berg et al., 2022; Berg et al., 2025; Janssen et al., 2022; Dupeyron et al., 2025). Applying our approach to these samples enables exploration of evolving speciation of C and S speciation in a rapidly changing lacustrine environment. Sediment samples for TGA/DSC-MicroGC were obtained from archived freeze-dried material.

2.2 Instrumentation and ultra-fast configuration mode

We coupled a TGA/DSC 3+ (Mettler Toledo) with a MicroGC (SRA Instruments) (Fig. 1) and calibrated the integrated system for precise, semi-continuous H, C and S analysis (Fig. 3). The TGA/DSC simultaneously monitors mass and heat flow changes as a function of temperature within a programmable continuous-flow gas-mixing furnace. The MicroGC, an ultra-fast gas chromatograph, separates, identifies, and quantifies light volatile compounds (e.g, H_2O, O_2, CH_4, CO_2, H_2S, COS and SO_2) present in the evolving gas mixture. In our hybrid setup, samples are heated in a programmable furnace at 10°C min^{-1} from 100-1000°C under a controlled atmospheres (typically 10 mL min^{-1} N_2 and 1 mL min^{-1} O_2). A secondary oxidation oven downstream of the primary furnace (maintained between 300-800°C) ensures complete oxidation of volatile species across the entire heating ramp. All carrier gases (N_2, O_2 and He) are of ultra-high purity (> 5.8; Carbagas and Linde). Evolved gases are transferred via a heated transfer line (80°C) to the MicroGC, equipped with Molsieve 5Å (for N_2, O_2) and PORAPLOT PPU (for CO_2, H_2S and SO_2) columns for efficient separation and quantification. The integrated TGA/DSC-MicroGC analytical system thus provides simultaneous, temperature-resolved measurements of mass loss, heat flow, and gas composition enabling real-time characterization of oxidation and redox processes.

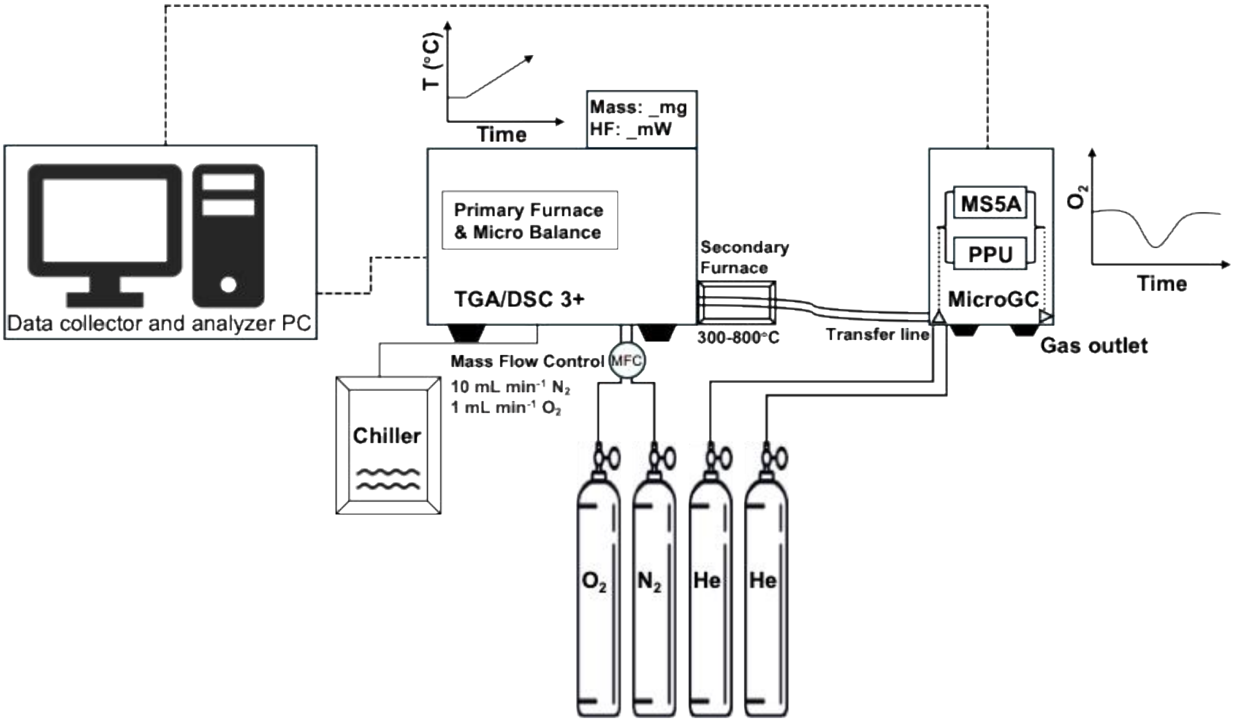

Figure 1. TGA/DSC-MicroGC instrument schematic.

2.3 Ultra-fast chromatographic mode

To resolve discrete devolatilization events of natural materials, we configured our Agilent Micro GC990 (Solia) system for a unique, ultra-fast dual-channel operation with a total cycle time of 54 second (15 s sampling and 39 s chromatographic run). Indeed, our target was not perfect peak separation of light hydrocarbons-as is typically prioritized in chromatography in cycles lasting over two minutes-but maximal temporal point density to capture the dynamic devolatilization profiles of light molecules with high resolution. The following ultra-fast MicroGC configuration prioritized cycle speed, and also resulted in excellent peak separation:

Channel A employed an MS5A SS column (10 m × 0.25 mm) held at 100 °C and 2.30 bar He pressure, with 90 °C injector heating, 15 ms injection time for sharp sample introduction, and backflush initiation after 13 s of chromatography to purge retained species; this setup optimized rapid separation and detection of permanent gases (O_2, N_2, CO) via thermal conductivity detection (TCD). Channel B used a PORAPLOT U FS column (10 m × 0.32 mm) maintained at 98 °C and 2.30 bar column pressure, with 90 °C injector, 50 ms injection to ensure adequate loading of less volatile analytes, and backflush set after 10 s; this enabled fast elution and quantification of CO_2, H_2S, H_2O, and SO_2. This specific configuration—refined by trial and error—delivered one complete gas composition data point every 54 s, generating approximately 100 high-density data points during a typical 90-minute experiment—sufficient to capture transient volatile release profiles with high temporal resolution.

2.4 Data Processing

Thermograms and calorimetric data were processed using STARe software. MicroGC chromatograms were analyzed with Solia, which quantified gas concentrations via external calibration (Fig. 3).

3 Results

3.1 Method Validation: Thermal Signatures and Calibration

The integrated analytical system produces distinct thermal decomposition signatures for a range of C- and S-bearing standards, allowing precise characterization of their molecular speciation (Fig. 2). Organic standards, such as L-cystine and cellulose, exhibited multi-stage decomposition profiles (Fig. 2A, B). L-cystine, a sulfur-rich amino acid, decomposed between 200°C and 700°C, releasing CO_2, H_2S, and COS (Fig. 2), where cellulose pyrolyzed between 250°C and 600°C, releasing primarily CO_2 and H_2O. The IFP standard displays overlapping mass-loss events, likely reflecting the concurrent oxidation of both organic and inorganic carbon phases (Fig. 2C, J). In contrast, inorganic standards yielded sharper and more distinct thermal spectra. Calcium carbonate ($CaCO_3$), for instance, exhibited a single, well-defined 44% mass loss between 600°C and 800°C, consistent with its thermal decomposition into CaO and CO_2 (Fig. 2D, K).

https://doi.org/10.5194/egusphere-2026-321
Preprint. Discussion started: 4 February 2026

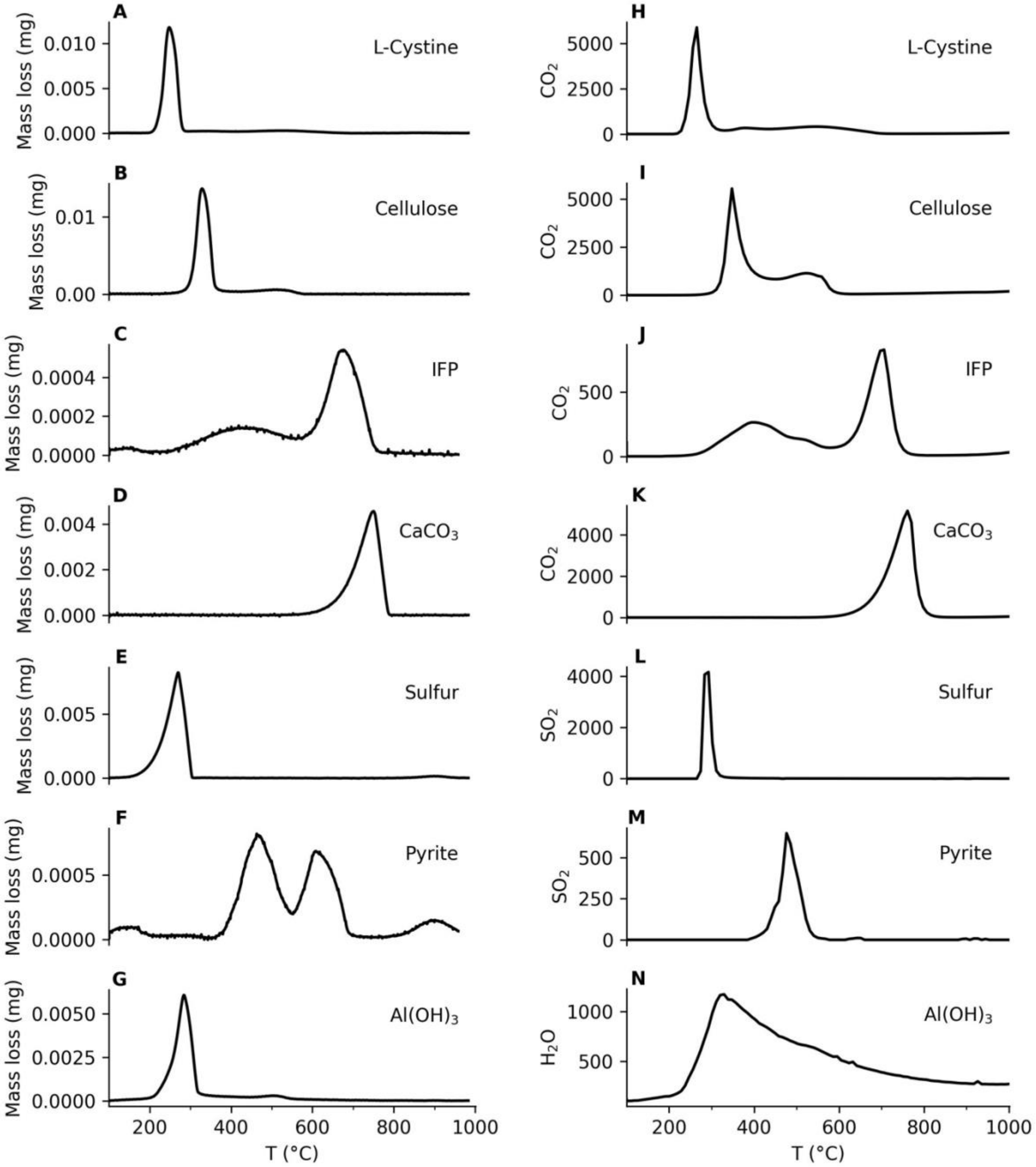

Figure 2. Mass loss and devolatilized components from standards evaluated by using TGA/DSC-MicroGC system. (A,
115 **H**) L-Cystine; (**B, I**) Cellulose; (**C, J**) IFP; (**D, K**) $CaCO_3$; (**E, L**) Elemental sulfur; (**F, M**) Pyrite; (**G, N**) $Al(OH)_3$.

Elemental S underwent rapid volatilization and oxidation between 100°C and 300°C under both non-oxidative and oxidative conditions (Fig. 2E, L). In contrast, pyrite (FeS_2) showed a distinct oxidative mass loss between 400°C and 600°C, corresponding to its conversion to Fe_2O_3 and release of SO_2 (Fig. 2F, M). Aluminium hydroxide [$Al(OH)_3$] released structural water (~13% mass loss) between 200°C and 300°C as it dehydrated to Al_2O_3 (Fig. 2G, N). The combined TGA/DSC-MicroGC profiles thus allow differentiation between organic and inorganic C and between organic and inorganic S species, based on their unique thermal decomposition kinetics and characteristic gas-phase reaction products. This capability provides a kinetically resolved and molecularly specific view of redox-active phases, an analytical resolution that is not achievable with conventional bulk techniques.

This hybrid system can also be operated in oxidation mode, enabling accurate quantification of total H, C and S concentrations. Under these conditions, all reactive species are completely oxidized to H_2O, CO_2 and SO_2, respectively, allowing for direct measurement of total element content. H_2O calibration was achieved through controlled dehydration of [$Al(OH)_3$], which releases a stoichiometric amount of water (Fig. 3A). Calibration for CO_2 employed certified reference materials, including industrial synthetic vitreous carbon and natural graphite, which were combusted in the oxidation mode to produce CO_2, and pure calcium carbonate ($CaCO_3$), which decomposed into CaO and CO_2. Additional calibration checks used ambient air with a known CO_2 concentration (427 ppm) and an IFP standard (Fig. 3B). Calibration for S species was performed using the oxidation of pyrite, IFP, CLB and JSD standards, yielding well-defined SO_2 peak (Fig. 3C). The resulting calibration curves for H_2O, CO_2 and SO_2 exhibit excellent linearity (R^2 >0.99, Fig. 3), confirming the robustness and precision of quantitative measurements under oxidation mode.

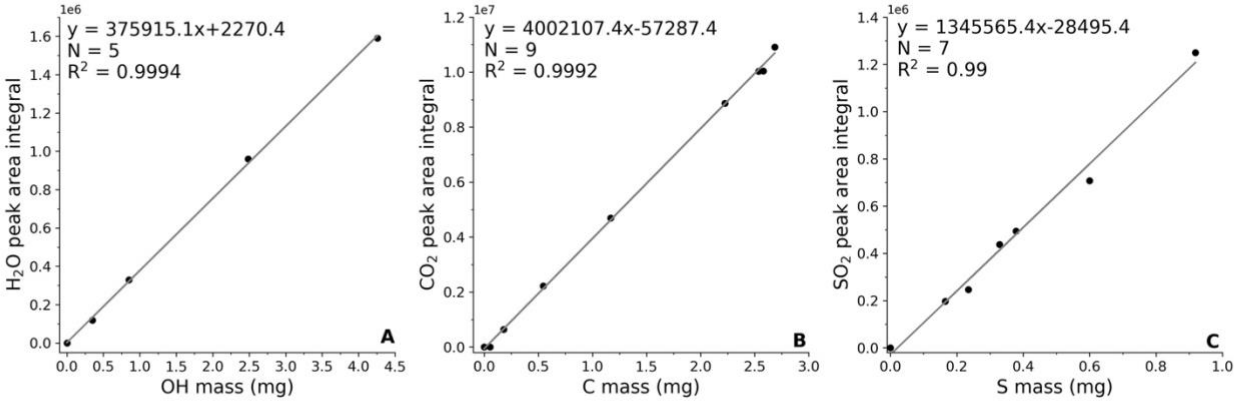

Figure 3. Calibrations. A, Hydrogen; **B,** Carbon; **C,** Sulfur.

3.2 Kinetically-resolved Characterization of Carbon and Sulfur in Natural Samples

Bulk mass-loss measurement alone does not capture the intrinsic reactivity of complex materials. To overcome this limitation, our approach uses pyrograms as a direct measure of the kinetics of C and S devolatilization and/or combustion pathways following Arrhenius law (Equation 1).

$$k = A\exp\left(-\frac{Ea}{RT}\right), \tag{1}$$

where k is the temperature-dependent rate constant, A is the empirically derived Arrhenius pre-exponential (“frequency”) factor, E_a is the activation energy, R is the ideal gas constant, and T is the measured temperature (see Table 1 for symbol descriptions).

Apparent activation energy (aE_a) were determined using a model-free isoconversional method of Vyazovkin (Vyazovkin and Wight, 1999), implemented in the STARe software. We compared the results with those obtained using a distributed activation energy model (DAEM) following (Hemingway et al., 2017). The pre-exponential factor was iteratively optimized (10^5 to 10^{12} s^{-1}) to ensure consistency between both methods, as a fixed A values led to systematic overestimation for certain standards (Fig. 4D, H). This optimized protocol was subsequently applied to natural samples.

https://doi.org/10.5194/egusphere-2026-321
Preprint. Discussion started: 4 February 2026

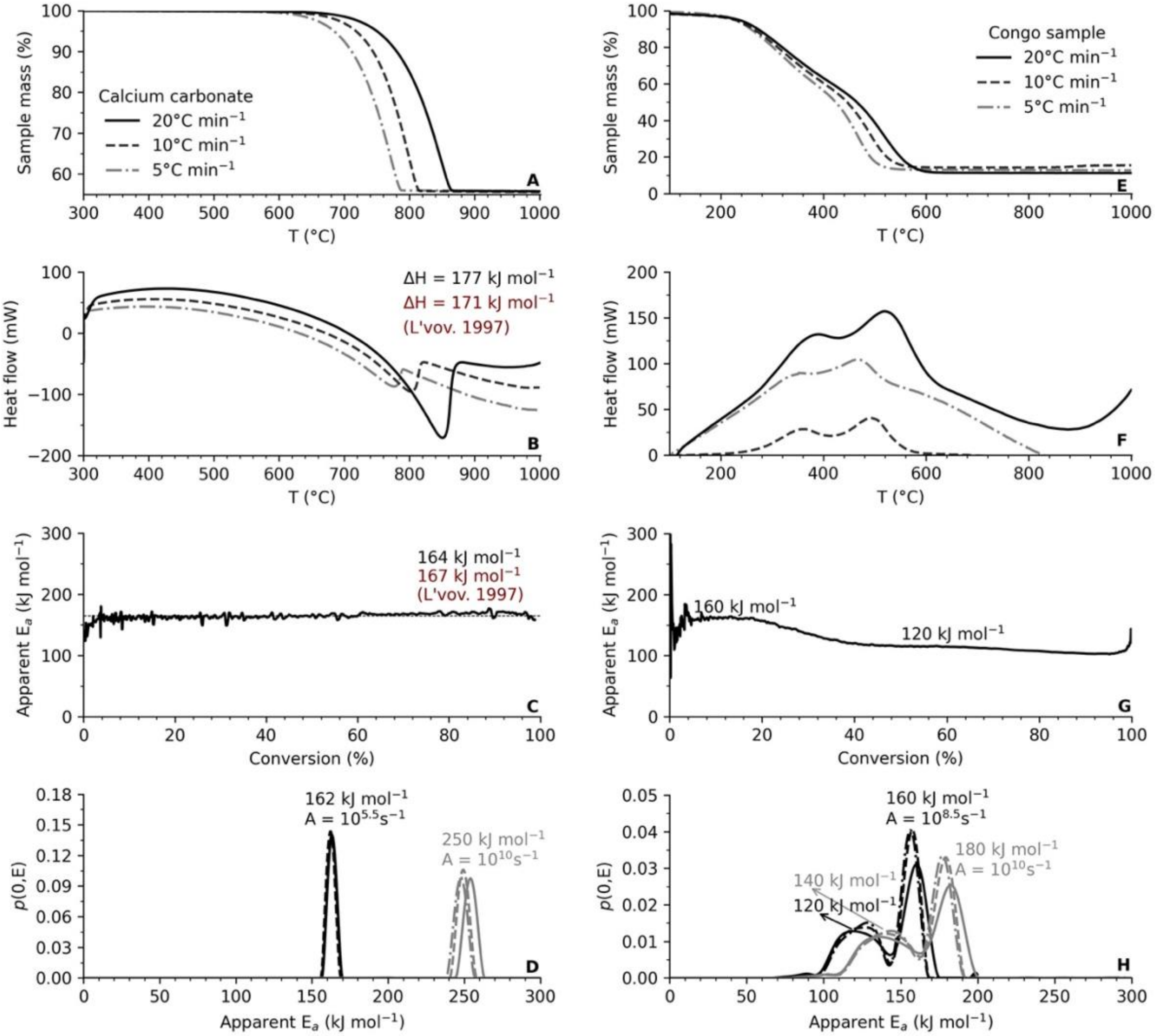

Figure 4. Thermal properties for standard calcium carbonate (left) and natural sample from Congo basin (right). (**A, E**) Mass loss curves from thermogravimetric analysis (TGA) at heating rates of 5, 10, and 20°C min^{-1}; (**B, F**) Corresponding heat flow profiles from differential scanning calorimetry (DSC); (**C, G**) Apparent activation energy (aE_a) as a function of conversion determined via the model-free isoconversional method (Vyazovkin and Wight, 1999); (**D, H**) Apparent activation energy distribution $p(0,E)$ derived from the distributed activation energy model (DAEM) for various pre-exponential factors (A) following (Hemingway et al., 2017).

To test the kinetic approach, we first analyzed $CaCO_3$ (99.9% purity) using the model-free isoconversional method (Fig. 4A-D). The method yielded a reaction enthalpy (ΔH) of 177 kJ mol^{-1} and aE_a of 164 kJ mol^{-1}, both consistent with published values(L'vov, 1997). In contrast, the DAEM with a fixed pre-exponential factor (A = 10^{10} s^{-1}) produced an overestimated aE_a of ~250 kJ mol^{-1}. Adjusting A to $10^{5.5}$ s^{-1} resulted the aE_a to 162 kJ mol^{-1}, closely matching the isoconversional and literature values (Fig. 4D). Applying the sample approach to a natural sediment sample from the Congo Basin (Fig. 4E-H) revealed two distinct aE_a at 160 kJ mol^{-1} and 120 kJ mol^{-1}, consistent with a two-step decomposition process likely reflecting different organic matter fractions. The DAEM with fixed A = 10^{10} s^{-1} again overestimated activation energies (~180 kJ mol^{-1} and 140 kJ mol^{-1}), while optimization to A = $10^{8.5}$ s^{-1} yielded values comparable to the isoconversional results. These confirm that dynamic adjustment of A is critical for accurately parametrizing the heterogeneous natural materials, particularly those containing mixed organic and mineral phases.

Thermograms of peatland sediment from the Congo Basin reveal two predominant organic fractions: a labile component (L) with a decomposition peak near 370°C and an aE_a of ~120 kJ mol^{-1}, and a refractory fraction (R), likely composed of aged lignocellulosic aromatic compounds, peaking at 500°C with an aE_a of ~160 kJ mol^{-1} (Fig. 5A). The ratio of the labile-to-refractory peak areas (L/R) increases markedly following peat initiation, indicating a higher proportion of thermally labile material. This substantial increase suggests either a shift in organic matter sources and/or enhanced preservation of labile compounds within the peat profile, consistent with independent paleoenvironmental proxies that pointing to a transition to wetter conditions that promoted peat accumulation and selective preservation of labile organic matter (Garcin et al., 2022).

Similarly, thermograms from Lake Cadagno sediments reveal three distinct sulfur fractions. Hydrogen sulfide (H_2S) and carbonyl sulfide (COS) evolved at low temperatures, with aE_a values of approximately 110 kJ $mol^{-1}$and 130 kJ mol^{-1}, respectively, consistent with the decomposition of labile organic sulfur compounds, such as thiols, sulfides, and disulfides, associated with fresh organic matter (Fig. 5B). A higher temperature SO_2 peak with an aE_a value of approximately 150 kJ mol^{-1} reflects the oxidative decomposition of pyrite (FeS_2). This differentiation clearly separates organic sulfur compounds from inorganic sulfide minerals, a resolution not achievable by conventional methods. The low-temperature release of H_2S and COS

https://doi.org/10.5194/egusphere-2026-321
Preprint. Discussion started: 4 February 2026

provides a kinetic fingerprint of dissimilatory sulfate reduction (DSR), the dominant anaerobic microbial pathway for S cycling in the lake's euxinic bottom waters. Conversely, the higher-temperature SO_2 peak reflects the thermal stability of pyrite, the end product of long-term biological DSR and diagenetic mineralization. Together, these results demonstrate that the TGA/DSC-MicroGC approach yields quantitative, kinetically resolved signatures of microbial and geochemical S transformations, linking molecular-scale reactivity to environmental processes.

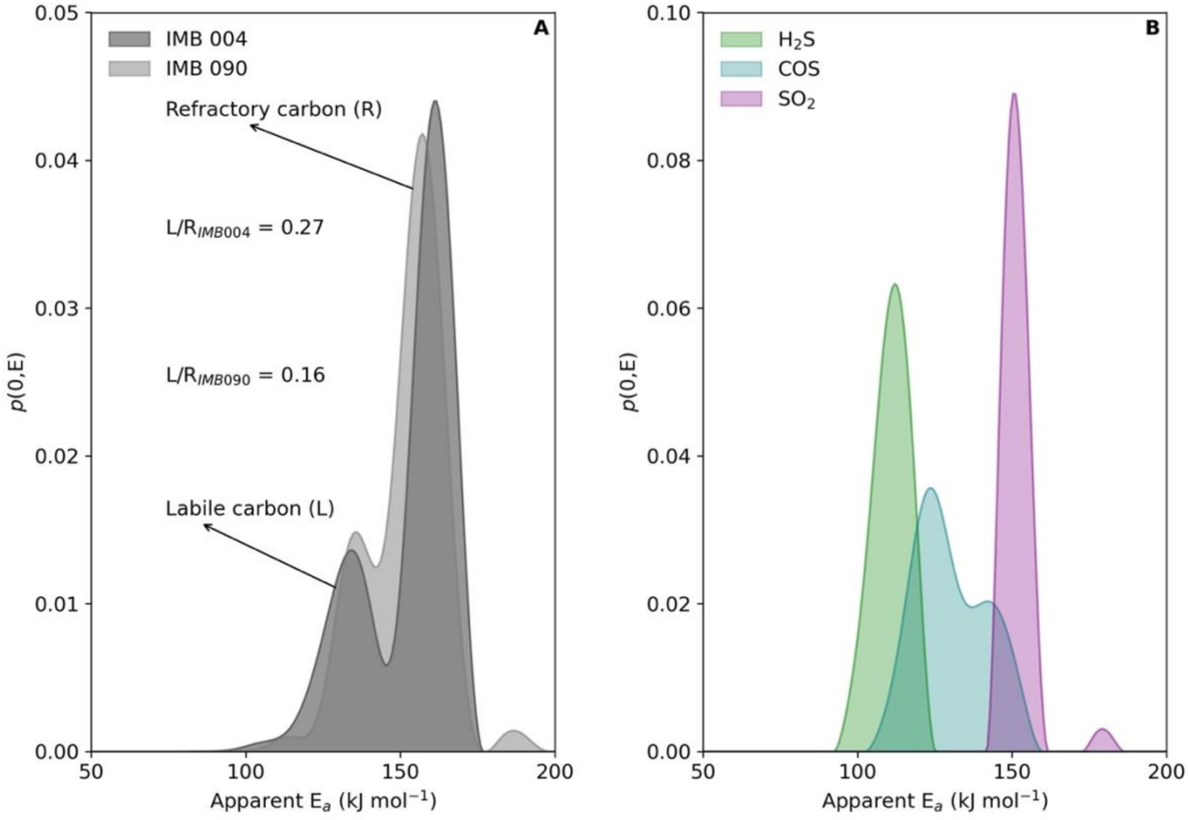

Figure 5. Kinetically-resolved carbon and sulfur speciation. A, aE_a distributions for carbon speciation in samples from the Congo Basin, including labile and refractory carbon fractions. **B**, aE_a distributions of sulfur speciation in a sample from Cadagno Lake, including H_2S, COS, and SO_2.

3.3 Absolute Redox Capacity and Oxidation Profiles

Having established the capacity to kinetically resolve individual species, we next address a more integrated property–the specific redox capacity (dO_2). To move beyond thermodynamic proxies and bulk speciation, we developed a method to quantify dO_2 through real-time monitoring of oxygen consumption during heating. Previous work introduced a high-temperature chalcometric technique, which determines total redox capacity by measuring oxygen exchange between a solid-state donor and the sample under vacuum (Galvez and Jaccard, 2021). Although highly effective for quantifying total oxygen demand, this earlier approach is limited to endpoint measurements provides no kinetic resolution and cannot distinguish the element-specific contributions to overall redox behavior.

Our method overcomes these limitations by continuously measuring O_2 concentrations in situ during the heating ramp. Samples are heated at a controlled rate (e.g. 10 °C min^{-1}), under a specific gas mixture, inducing progressive devolatilization and oxidation while the MicroGC continuously monitors evolving gas compositions. The decline in the O_2 concentrations is integrated over time to calculate the cumulative volume of O_2 consumed, normalized to the initial sample mass and the stoichiometric oxidation reactions (Fig. 6A). This method yields highly reproducible measurements of absolute redox capacity with a relative standard deviation of 0.82% for vitreous carbon standards (Fig. 6B). Importantly, our results accurately reproduces those obtained by the vacuum line protocol (Galvez and Jaccard, 2021), validating the precision and robustness of this continuous, kinetically resolved redox quantification method.

Redox capacity (dO_2) was calculated as:

i. Volume of O_2 supply (V_{sup})

$$V_{sup} = f \times \Delta t, \tag{2}$$

where f is the O_2 flow rate (1 ml min^{-1}) and Δt is time interval.

ii. Volume of O_2 consumed (V_{con})

$$V_{con} = \frac{\int_{t1}^{t2} A_{eff}\, dt}{\int_{t1}^{t2} A_{tot}\, dt} \times V_{sup}\,, \tag{3}$$

where A_{eff} is time-integrated effective area corresponding to consumed O_2 and A_{tot} is time-integrated total area.

iii. Redox capacity (dO_2)

$$dO_2 = \frac{PV_{con}}{RT \times m}, \quad (4)$$

where P is gas pressure, R is the ideal gas constant, T is the room temperature and m indicates sample mass.

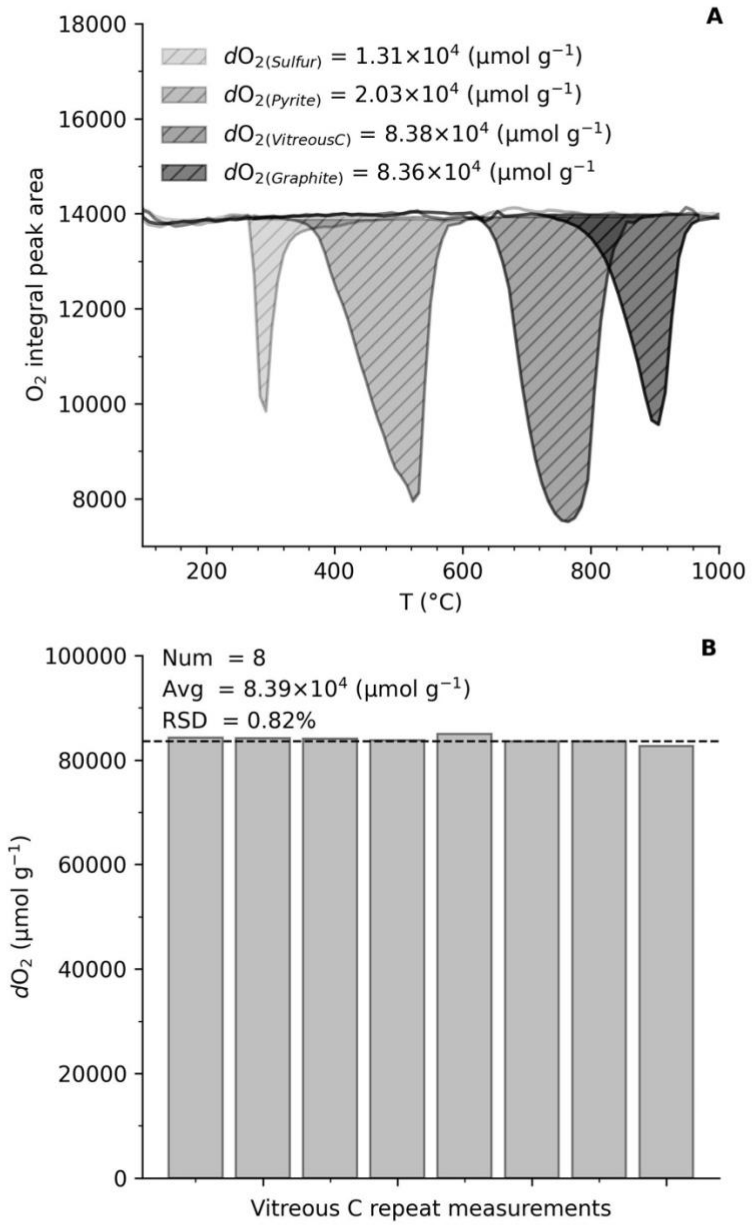

Figure 6. Redox capacity. A, Oxygen profiles of sulfur, pyrite, Vitreous C and graphite along with temperature; **B**, Repeat measurements for standand Vitreous C with relative standard deviation (RSD = 0.82%), indicating high precision and reproducibility. Black dashed lines indicate the theoretical value.

The oxidation of various standards was examined to validate this new continuous dO_2 protocol. The measured dO_2 values for elemental sulfur ($dO_2 = 1.31 \times 10^4$ µmol g^{-1}) and pyrite ($dO_2 = 2.03 \times 10^4$ µmol g^{-1}) are approximately 40% and 11% lower, respectively, than their theoretical values (3.13×10^4 and 2.29×10^4 µmol g^{-1}). We attribute these discrepancies to premature, non-oxidative S volatilization during heating, which prevents complete oxidation within the experimental timeframe. In contrast, both vitreous carbon ($dO_2 = 8.38 \times 10^4$ µmol g^{-1}) and natural graphite (8.36×10^4 µmol g^{-1}) display excellent alignment with theoretical predictions (8.36×10^4 µmol g^{-1}). Their oxidation occurs at higher temperatures (>400°C), where losses due to non-oxidative volatilization are minimal, confirming the method's precision and quantitative accuracy for refractory minerals.

A significant advantage of this novel method is that it quantifies the absolute redox capacity of a material independent of its redox history. By continuously tracking oxygen consumption throughout controlled heating, the method captures the total reducible inventory of a sample, the cumulative amount of material capable of electron exchange when exposed to an oxygen-rich atmosphere (Fig. 6). The integrated O_2 consumption across the entire temperature range thus provides a comprehensive measure of intrinsic redox capacity, reflecting a fundamental property of the material rather than a transient environmental state.

3.4 Secondary oven and optimization to complete oxidation

To address the incomplete oxidation of volatile S and light hydrocarbon species, we introduced a secondary oven downstream of the primary heating chamber (Fig. 1). The oven is held at a constant, adjustable temperature (300-800°C), ensuring that volatile intermediates (e.g., S vapor, reduced hydrocarbons) remain in the gas stream long enough to undergo complete oxidation (Fig. 7A) independent of the upstream heating rate and temperature. Measurements on standards including elemental S and pyrite confirm that the secondary oven significantly improve the oxidation efficiency (Fig. 7B, C). For instance, the *d*O_2 of pyrite increases from 2.03 × 10^4 µmol g^{-1} (without secondary oven) to 2.28 × 10^4 µmol g^{-1}, when the secondary oven was maintained at 800°C, corresponding to 95–99% of theoretical oxidation capacity (Fig. 7C). Similarly, elemental S and other S-bearing standards displayed consistent increases in *d*O_2 with rising secondary oven temperatures (Fig. 7B). Natural samples from the black shales, Lake Cadagno sediments, and Congo peat also showed systematic *d*O_2 increases of 10–20% with an 800°C secondary oven (Fig. 7D-F). These results underscore the critical role of secondary heating in mitigating the low-temperature volatilization losses, particularly for sulfur- and fresh organic-rich materials. The implementation of a secondary oven thus ensures quantitative oxidation of volatile phases and enhances the accuracy and reproducibility absolute redox capacity measurements.

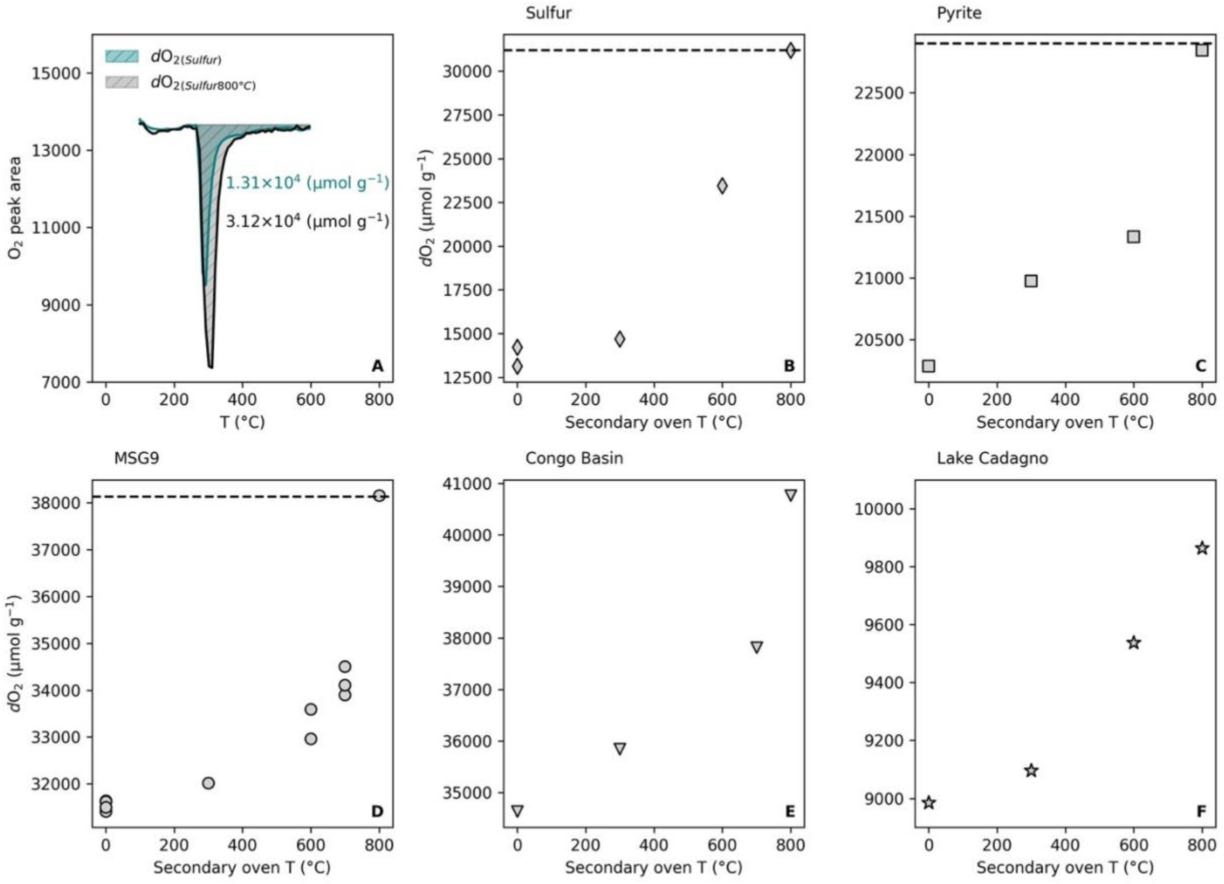

Figure 7. Optimized redox capacity with secondary oven. A, Comparison of elemental sulfur measurements with secondary oven (at 800°C, grey) and without secondary oven (teal); **B**, Elemental sulfur; **C**, Pyrite; **D**, Black shale (MSG9); **E**, Peat sediment from the Congo basin; **F**, Lake Cadagno sediment. Black dashed lines in B, C and D panels indicate the theoretical values.

4 Kinetic fingerprints

4.1 Oxygen consumption and redox-active components

Beyond quantifying total redox capacity, our approach yields kinetically resolved oxygen consumption profiles, offering a distinctive "redox fingerprint" of reducible components in complex matrices. The Congo Basin sample exhibits a dual oxidation pattern: ~36.9% of the total O_2 attributed to labile organic matter oxidizing at 250–450 °C, while the dominant fraction (63.1%) associated with refractory organic matter oxidizing above 500 °C (Fig. 8A). These two stages are consistent with broad CO_2 peaks observed in the gas evolution data (Fig. 8D), confirming the contrasting thermal stability of organic matter pools. The Lake Cadagno sediment exhibits a mixed organic C–S oxidation signature, with 38.0% of the total O_2 uptake derived from organic C and S-bearing compounds, and 62.0% associated with refractory C and pyrite oxidation, extending to 700 °C (Fig. 8B). The synchronous evolution of CO_2, SO_2, COS, H_2S (Fig. 8E), reflects coupled oxidation of sulfurized organic matter and pyrite, highlighting microbially mediated sulfurization and its long-term preservation in the sedimentary record. In contrast, the fayalite standard is dominated by Fe(II) oxidation, which accounts for 88.1% of the total O_2 consumption at high temperatures (500-900°C), with only 11.9% originates from minor organic matter oxidation (Fig. 8C). This is consistent with a weak low-temperature CO_2 peak and illustrates the method's ability to distinguish metal-driven versus organic-driven redox processes (Fig. 8C, F).

Together, these results demonstrate that integrating O_2 consumption profile with simultaneous gas evolution enables the quantitative partitioning of oxygen demand among labile organic matter, refractory carbon, sulfur-bearing phases, and Fe(II) minerals, providing a comprehensive kinetic redox characterization of the thermal reactivity of sediments and minerals.

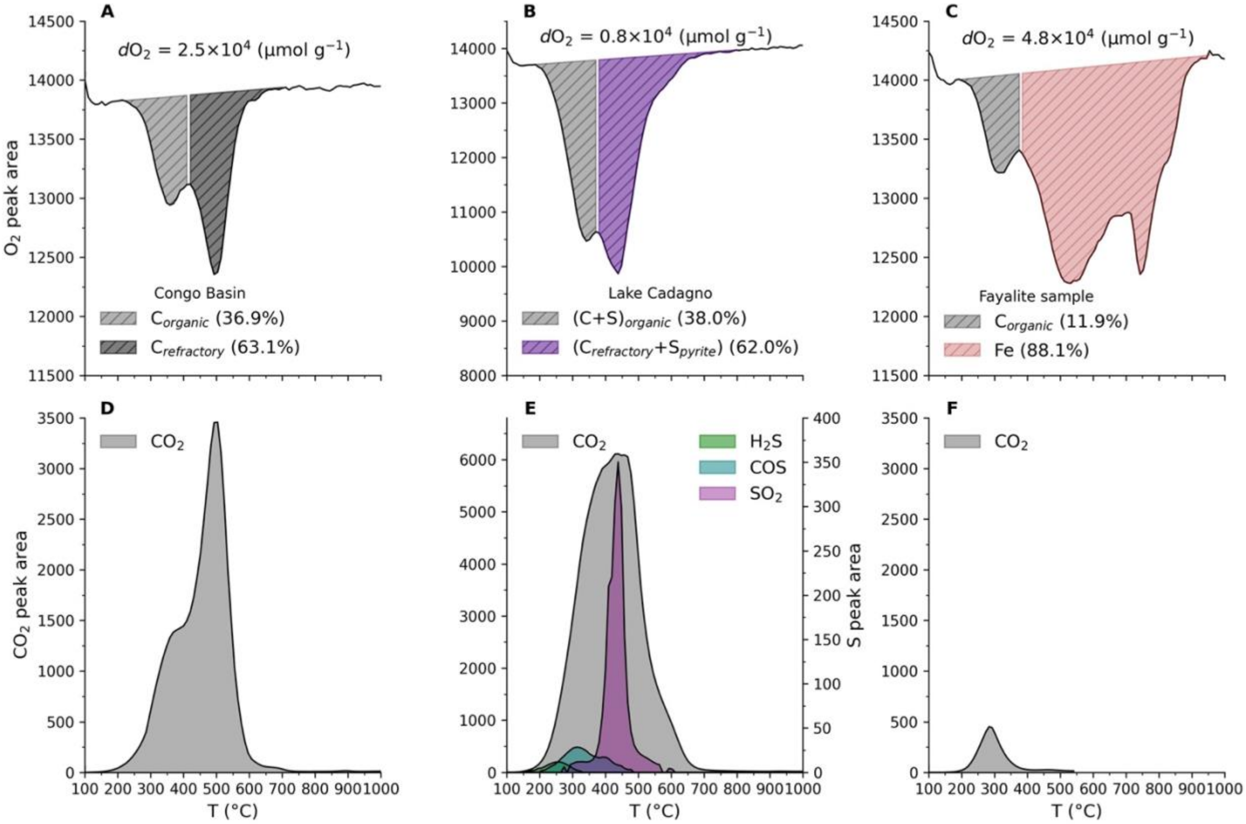

Figure 8. Oxidation profile with corresponding components. **A**, Congo Basin peat sample; **B**, Cadagno Lake sediment sample; **C**, Fayalite sample; **D-F**, Gases released through distinct reactions from samples A, B and C, respectively.

4.2 Sulfur cycle and Diagenesis in Cadagno Lake

To further demonstrate the capabilities of our method, we applied it to a sediment profile from Lake Cadagno, a well-known system for studying microbial sulfur cycling and diagenetic processes (Berg et al., 2022; Berg et al., 2025; Dupeyron et al., 2025).

Our results reveal a distinct redox transition marked by a progressive decline in dO_2 and total organic carbon (TOC) with depth, while COS and H_2S signals persist throughout the profile (Fig. 9A-D). In contrast, SO_2 concentrations are low near the surface, increase sharply to a maximum around 18-20 cm, and then decline toward to the base of the core (Fig. 9E). This hump-shaped SO_2 pattern identifies a zone of intense S remobilization and re-oxidation, coinciding with the microbial redox transition zone where sulfate reduction peaks.

The aE_a spectra, derived from the SO_2 release kinetics, provide a deeper view into the progression of S diagenesis. In the upper zone (7-15 cm), the spectra exhibit multiple peaks spanning 80-240 kJ mol^{-1}, reflecting a heterogeneous assemblage of metastable metal sulfides such as ZnS, $Fe_{1-x}S$, and PbS (Fig. 9F). In the transitional middle zone (15-19 cm), the spectra simplify to three partially overlapping peaks, indicating progressive loss of the most labile sulfide phases and partial transformation (Fig. 9G). Below the 19-20 cm boundary, the spectra converge into a single dominant peak at approximately 140-160 kJ mol^{-1}, consistent with the formation of thermally stable pyrite (FeS_2) (Fig. 9H). This clear diagenetic transition from diverse, reactive sulfides to a single, uniform phases of pyrite highlight the multi-stage and progressive nature of sulfur mineral maturation in anoxic sediments.

We interpret the 19-20 cm boundary as marking a sulfate-depletion front, where organic matter driven sulfate reduction in the upper sediment generates H_2S that precipitating transient metal sulfides, while deeper layers record the maturation of pyrite sustained by internal sulfur cycling under sulfate-limited conditions. The transformation into stable pyrite strengthens the long-term sulfur burial and reduces the pool of reactive sulfur species, potentially modulating redox balance, microbial metabolism and biodiversity in meromictic lake systems. By resolving activation energy distributions, our method provides a new kinetic framework tracking diagenetic fronts and reconstructing microbial sulfur cycling and redox transitions in anoxic environments, offering a powerful tool for paleoenvironmental and early diagenetic studies.

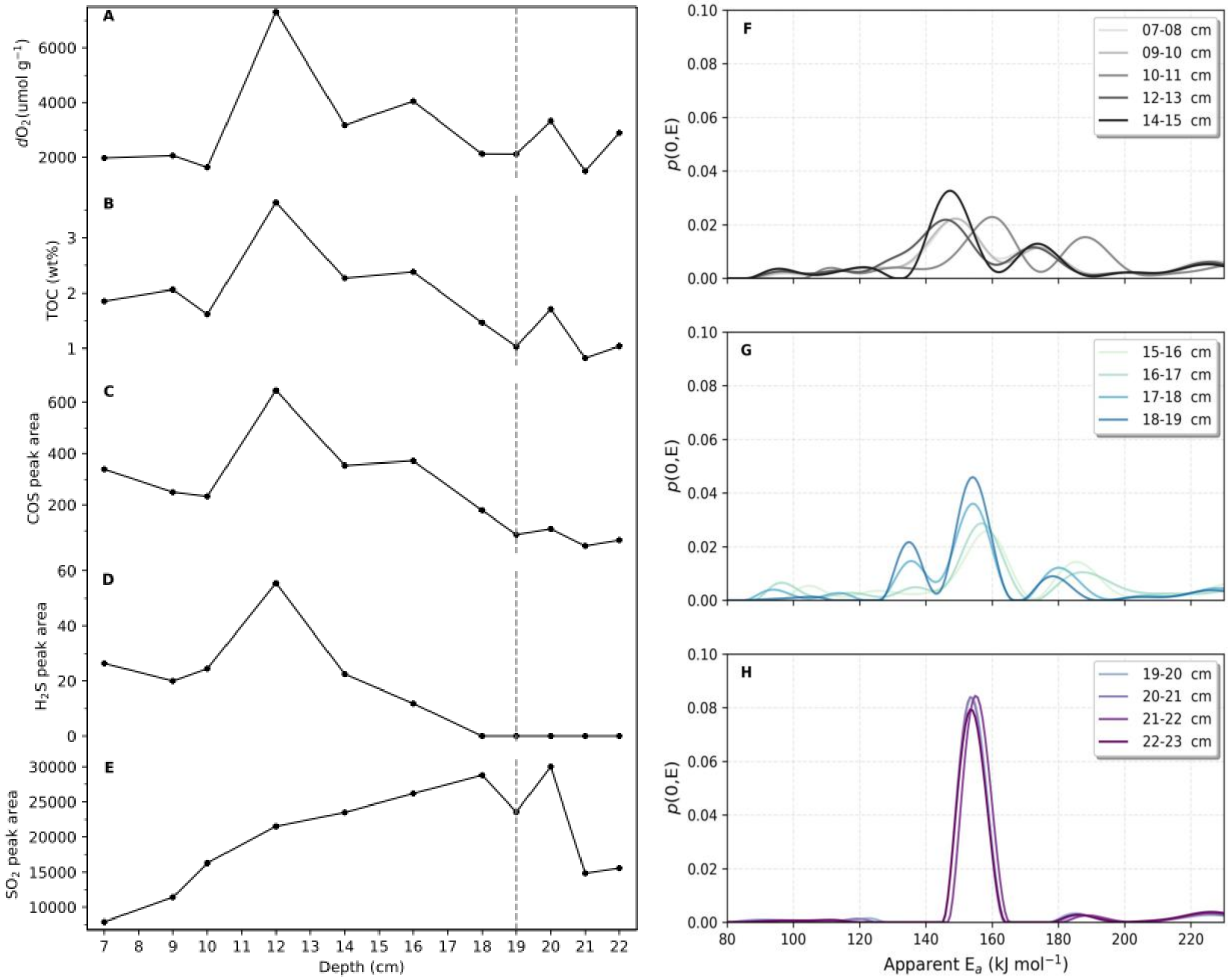

Figure 9. Cadagno Lake depth profile. **A**, dO_2; **B**, TOC content; **C**, COS; **D**, H_2S; **E**, SO_2; **F**, aE_a spectral distributions of SO_2 from the upper zone (7-15 cm); **G**, aE_a spectral distributions of SO_2 from the middle zone (15-19 cm). **H**, aE_a spectral distributions of SO_2 from the lower zone (19-22 cm). Dash line indicates the diagenetic boundary.

4.3 Kinetic fingerprint for materials: redox chemistry

The TGA/DSC-MicroGC platform delivers a unified kinetic fingerprint—a spectral signature of C, S, O, and H reactivity—captured in a single analytical run under controlled ramped oxidation. This kinetic fingerprint is exemplified in Fig. 10 for a representative sulfidic sediment from Lake Cadagno. It shows gradual sample mass loss corresponding heat flow profile, where exothermic features highlight bond cleavage and oxidation reactions (Fig. 10A, B). Moreover, it tracks the oxidation profile and evolved gases, revealing O_2 consumption alongside reduced components, including organic and mineral sulfur species and carbon (H_2S, COS, SO_2 and CO_2) (Fig. 10C, D and E). Last but not least, the apparent activation energy distribution shows low aE_a (~100–140 kJ mol^{-1}) for H_2S, COS indicating labile organic sulfur, monosulfides and carbon, while high aE_a (~150–180 kJ mol^{-1}) for SO_2, CO_2 reflecting refractory pyrite and carbon (Fig. 10F).

By synchronously resolving mass-loss kinetics, enthalpic transitions, activation energy distributions, and near-continuous evolved gas profiles (O_2, CO_2, H_2S, COS, SO_2) (Fig. 10), this approach resolves the molecular identity, thermal stability, and redox stoichiometry of every electron-transferring phase.

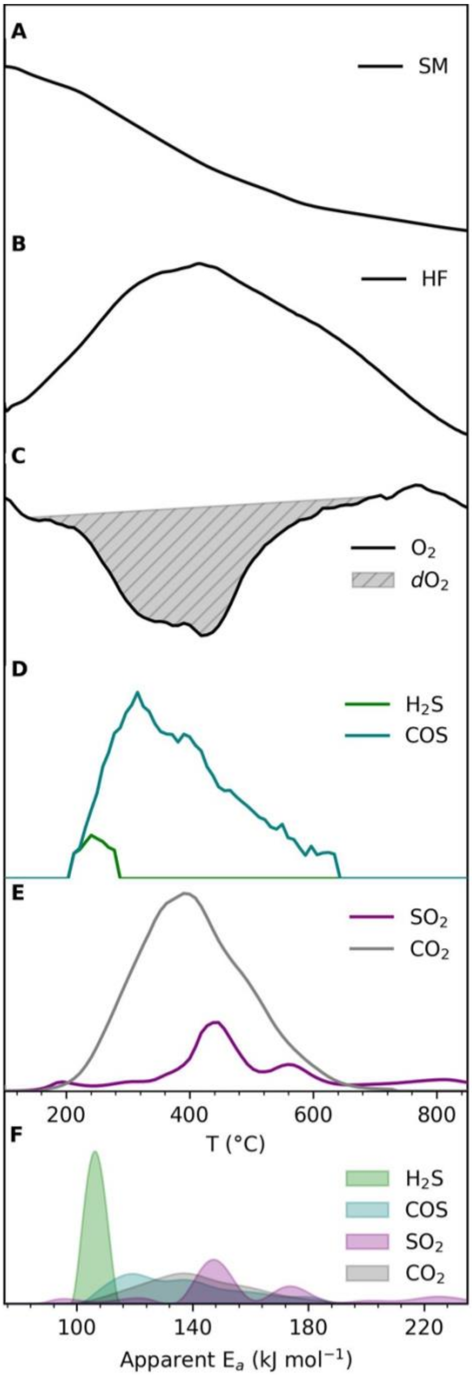

335

Figure 10. Kinetic fingerprint for a representative sulfidic sediment from Lake Cadagno. A, Sample mass (SM) changes at heating rates of 10°C min^{-1}; **B**, Heat flow (HF) profile; **C**, Oxidation profile; **D,** H_2S and COS profiles; **E**, SO_2 and CO_2 profiles; **F**, *aE_a* distribution of H_2S, COS, SO_2 and CO_2.

https://doi.org/10.5194/egusphere-2026-321
Preprint. Discussion started: 4 February 2026

5 Conclusions

In this study, we have developed and validated a novel, integrated TGA/DSC-MicroGC analytical system that offers unprecedented resolution of biogeochemical speciation and reactivity in geological materials. This method kinetically resolves the thermal decomposition of complex C and S species, inaccessible to conventional bulk analyses, while also enabling the quantification of absolute redox capacity and continuous kinetically resolved oxidation profiles.

Applications to natural archives from the Congo Basin and Lake Cadagno demonstrate the method's broad utility and transformative implications. In tropical peatland sediments, it allowed the quantification of paleo-oxygen fluxes linked to organic C burial (Galvez et al., 2025). In Lake Cadagno sediments, our results revealed a diagenetic front defined by a shift in sulfide speciation and apparent activation energy, providing a direct kinetic proxy for past microbial processes and redox evolution. Overall, this integrated approach moves beyond static bulk measurements toward a mechanistic, high-resolution framework for tracing coupled C-O-S dynamics in Earth materials. Future application to rocks, marine sediment, soils, meteorites, and other anoxic environments promise to advance our understanding of the co-evolution of life, climate and planetary redox balance.

Data availability

The data related to this study will be openly available in Zenodo.

Author contributions

Conceptualization: M.G., S.W.; Investigation: S.W., M.E.G.; Methodology: S.W., M.E.G. Writing – original draft: S.W.; Writing – review and editing: S.W., S.L.J., M.E.G.

Competing interests

The authors declare no competing financial interest.

Acknowledgements

This project was supported through Swiss National Science Foundation, 215097. We thank J. Dupeyron, J. M. Carbonne and Y. Garcin for proving the sediment samples from the Lake Cadagno and the Congo Basin as well as for their helpful discussions. S. W acknowledges funds from the Chinese Academy of Sciences-Pioneer Hundred Talents Program (grant E5710403). Funding from the Swiss National Science Foundation is acknowledged (grant 215097 to M.E.G. and grants 200021_163003 and 200020_192361 awarded to S.L.J.).

References

Alt, J. C. and Shanks Iii, W. C.: Stable isotope compositions of serpentinite seamounts in the Mariana forearc: Serpentinization processes, fluid sources and sulfur metasomatism, Earth Planet Sc Lett, 242, 272-285, 10.1016/j.epsl.2005.11.063, 2006.

Berg, J. S., Rodriguez, P. C., Magnabosco, C., Deng, L., Bernasconi, S. M., Vogel, H., Morlock, M., and Lever, M. A.: Active microbial sulfur cycling across a 13,500-year-old lake sediment record, EGUsphere, 2025, 1-27, 10.5194/egusphere-2024-4158, 2025.

Berg, J. S., Lepine, M., Laymand, E., Han, X., Vogel, H., Morlock, M. A., Gajendra, N., Gilli, A., Bernasconi, S. M., Schubert, C. J., Su, G., and Lever, M. A.: Ancient and Modern Geochemical Signatures in the 13,500-Year Sedimentary Record of Lake Cadagno, Front Earth Sc-Switz, Volume 9 - 2021, 10.3389/feart.2021.754888, 2022.

Boudreau, B. P.: A kinetic model for microbic organic-matter decomposition in marine sediments, FEMS Microbiology Ecology, 11, 1-14, 10.1111/j.1574-6968.1992.tb05789.x, 1992.

Carter, T. L., Schaecher, C., Monteith, S., and Ferguson, R.: Using combustion analysis to simultaneously measure soil organic and inorganic carbon, GEODERMA, 451, 10.1016/j.geoderma.2024.117066, 2024.

Cohen-Sadon, H., Amrani, A., Feinstein, S., and Rosenberg, Y. O.: A new empirical approach for rapid quantification of organic and pyritic sulfur in sedimentary rocks using the Rock-Eval 7S, Organic Geochemistry, 166, 104350, 10.1016/j.orggeochem.2021.104350, 2022.

Crezee, B., Dargie, G. C., Ewango, C. E. N., Mitchard, E. T. A., Emba B, O., Kanyama T, J., Bola, P., Ndjango, J.-B. N., Girkin, N. T., Bocko, Y. E., Ifo, S. A., Hubau, W., Seidensticker, D., Batumike, R., Imani, G., Cuní-Sanchez, A., Kiahtipes, C. A., Lebamba, J., Wotzka, H.-P., Bean, H., Baker, T. R., Baird, A. J., Boom, A., Morris, P. J., Page, S. E., Lawson, I. T., and Lewis, S. L.: Mapping peat thickness and carbon stocks of the central Congo Basin using field data, Nat Geosci, 15, 639-644, 10.1038/s41561-022-00966-7, 2022.

Dupeyron, J., Pasquier, V., Guibourdenche, L., Busigny, V., Cartigny, P., Jézéquel, D., Bernasconi, S. M., and Carbonne, J. M.: Decadal, sediment-driven sulfur isotope evolution in Lake Cadagno, Geochemical Perspectives Letters, 38, 17-22, https://doi.org/10.7185/geochemlet.2550, 2025.

Espitalie, J., Deroo, G., and Marquis, F.: Rock-Eval Pyrolysis and Its Applications (Part Two), Rev. Inst. Fr. Pét., 40, 755-784, 10.2516/ogst:1985045, 1985.

Galvez, M., Wu, S., Garcin, Y., Schefuß, E., Gassier, G., Lebamba, J., Kiahtipes, C., Bokomba, F., Wotzka, H. P., and Adatte, T.: Peatlands' O_2 Pulses: Time-resolved Terrestrial Oxygen Production in the Central Congo Basin over the Holocene, Nature Geoscience (under review), 10.21203/rs.3.rs-7398366/v1, 2025.

Galvez, M. E.: Redox constraints on a Cenozoic imbalance in the organic carbon cycle, American Journal of Science, 320, 730-751, 10.2475/10.2020.03, 2020.

Galvez, M. E. and Jaccard, S. L.: Redox capacity of rocks and sediments by high temperature chalcometric titration, Chemical Geology, 564, 120016, 10.1016/j.chemgeo.2020.120016, 2021.

Garcin, Y., Schefuß, E., Dargie, G. C., Hawthorne, D., Lawson, I. T., Sebag, D., Biddulph, G. E., Crezee, B., Bocko, Y. E., Ifo, S. A., Mampouya Wenina, Y. E., Mbemba, M., Ewango, C. E. N., Emba, O., Bola, P., Kanyama Tabu, J., Tyrrell, G., Young, D. M., Gassier, G., Girkin, N. T., Vane, C. H., Adatte, T., Baird, A. J., Boom, A., Gulliver, P., Morris, P. J., Page, S. E., Sjögersten, S., and Lewis, S. L.: Hydroclimatic vulnerability of peat carbon in the central Congo Basin, Nature, 612, 277-282, 10.1038/s41586-022-05389-3, 2022.

Hayes, J. M. and Waldbauer, J. R.: The carbon cycle and associated redox processes through time, Philosophical Transactions of the Royal Society B: Biological Sciences, 361, 931-950, 10.1098/rstb.2006.1840, 2006.

Hemingway, J. D., Rothman, D. H., Rosengard, S. Z., and Galy, V. V.: Technical note: An inverse method to relate organic carbon reactivity to isotope composition from serial oxidation, Biogeosciences, 14, 5099-5114, 10.5194/bg-14-5099-2017, 2017.

Hemingway, J. D., Hilton, R. G., Hovius, N., Eglinton, T. I., Haghipour, N., Wacker, L., Chen, M.-C., and Galy, V. V.: Microbial oxidation of lithospheric organic carbon in rapidly eroding tropical mountain soils, Science, 360, 209-212, 10.1126/science.aao6463, 2018.

Janssen, D. J., Rickli, J., Wille, M., Sepúlveda Steiner, O., Vogel, H., Dellwig, O., Berg, J. S., Bouffard, D., Lever, M. A., Hassler, C. S., and Jaccard, S. L.: Chromium Cycling in Redox-Stratified Basins Challenges δ53Cr Paleoredox Proxy Applications, Geophys Res Lett, 49, e2022GL099154, 10.1029/2022GL099154, 2022.

L'Vov, B. V.: Mechanism of thermal decomposition of alkaline-earth carbonates, Thermochimica Acta, 303, 161-170, 10.1016/S0040-6031(97)00261-X, 1997.

Ordoñez, L., Vogel, H., Sebag, D., Ariztegui, D., Adatte, T., Russell, J. M., Kallmeyer, J., Vuillemin, A., Friese, A., Crowe, S. A., Bauer, K. W., Simister, R., Henny, C., Nomosatryo, S., and Bijaksana, S.: Empowering conventional Rock-Eval pyrolysis for organic matter characterization of the siderite-rich sediments of Lake Towuti (Indonesia) using End-Member Analysis, Organic Geochemistry, 134, 32-44, 10.1016/j.orggeochem.2019.05.002, 2019.

Paytan, A., Kastner, M., Campbell, D., and Thiemens, M. H.: Sulfur Isotopic Composition of Cenozoic Seawater Sulfate, Science, 282, 1459-1462, 10.1126/science.282.5393.1459, 1998.

Salonen, K.: A versatile method for the rapid and accurate determination ofcarbon by high temperature combustion, LIMNOLOGY AND OCEANOGRAPHY, 24, 177-183, 10.4319/lo.1979.24.1.0177, 1979.

Sebag, D., Verrecchia, E. P., Cécillon, L., Adatte, T., Albrecht, R., Aubert, M., Bureau, F., Cailleau, G., Copard, Y., Decaens, T., Disnar, J. R., Hetényi, M., Nyilas, T., and Trombino, L.: Dynamics of soil organic matter based on new Rock-Eval indices, Geoderma, 284, 185-203, 10.1016/j.geoderma.2016.08.025, 2016.

Vyazovkin, S. and Wight, C. A.: Model-free and model-fitting approaches to kinetic analysis of isothermal and nonisothermal data, Thermochimica Acta, 340-341, 53-68, 10.1016/S0040-6031(99)00253-1, 1999.

Yoon, G., Park, S.-M., Yang, H., Tsang, D. C. W., Alessi, D. S., and Baek, K.: Selection criteria for oxidation method in total organic carbon measurement, Chemosphere, 199, 453-458, 10.1016/j.chemosphere.2018.02.074, 2018.

435 Zhao, W. Z., Lu, B., Lv, S. N., Zhou, C. F., and Yang, Y.: Simultaneous determination of chlorine and sulfur in geochemical reference samples by wavelength dispersive X-ray fluorescence spectrometry, NEW JOURNAL OF CHEMISTRY, 44, 11224-11230, 10.1039/d0nj02042g, 2020.